Supplementary materials

Conjugated microporous polytriphenylamine as high-performance anion-capture electrode for hybrid capacitive deionization with ultrahigh areal adsorption capacity

Weiqing Kong*[a], Xiaoyuan Lu [a], Xu Ge [a], Qingao Zhang [a], Xiaoyu Jin [a], Meng Zhang [a], Yuanyuan Feng*[a]

[a] Key Laboratory of Catalytic Conversion and Clean Energy in Universities of Shandong Province, College of Chemistry and Chemical Engineering, Qufu Normal University, Qufu, Shandong 273165, PR China

* E-mail addresses: hxkwq3069@163.com; fengyy@qfnu.edu.cn

Experimental Section

Chemicals: All chemical reagents used in this work were of analytical grade in purity and commercially available. They were used directly without any further purification.

Synthesis of m-PTPA and n-PTPA: m-PTPA was synthesized via Buchwald–Hartwig cross-coupling of TAPA and TBPA monomers with the presence of inorganic salt KBr, as was described previously.[1-3] Briefly, 0.5 mmol tris(4-bromophenyl)amine, 0.75 mmol Tris(4-aminophenyl)amine, 0.03 mmol bis(dibenzylideneacetone)palladium, 0.045 mmol 2-dicyclohexylphosphino-2',4',6'-triisopropylbiphenyl, 2 mmol sodium tert-butoxide, 0.5 mmol KBr, 15 mL 1,4-dioxane, and 15 mL toluene were mixed and stirred for 15 min under an N_2 atmosphere in a 100 ml Schlenk tube. Subsequently, the Schlenk tube undergo freeze-pump-thaw cycles for three times to completely removed the remaining oxygen, then filled with N_2 and heated at 70 °C for 24 h. The final reaction mixture was washed by chloroform, hot deionized water, and methanol, followed by Soxhlet extraction with methanol for 24 h. Finally, the purified m-PTPA powder was dried for 12 h at 60 °C under vacuum conditions.

The synthetic procedure of non-microporous polytriphenylamine (n-PTPA) was the same as that of m-PTPA but without the addition of KBr.

Characterization: Scanning electron microscopy (SEM) and transmission electron microscopy (TEM) images, along with Fourier-transform infrared (FT-IR) spectra, were obtained using a ∑IGMA microscope (Zeiss, Germany) and a JEM-2100F microscope (JEOL, Japan), and an IRTracer-100 spectrometer (Shimadzu, Japan) with a KBr pellet, respectively. X-ray photoelectron spectra (XPS) was acquired using a SCALAB 250Xi spectrometer (Thermo Fisher Scientific, America) and calibrated by aligning C 1s peak to 284.6 eV. X-ray diffractometer (XRD) patterns were recorded on a MiniFlex-600 X-ray diffractometer (Rigaku, Japan) operating at 30 kV, 10 mA, and a scanning rate of 10°/min using Cu Kα radiation (0.15406 nm). N_2 adsorption-desorption isotherms were measured on an ASAP 2020 analyzer (Micromeritics,

America) at 77 K, and the corresponding specific surface area and the pore size distribution were estimated using the Brunauer-Emmett-Teller (BET) method and Barrett-Joyner-Halenda (BJH) method, respectively.

Electrochemical and desalination tests: The Electrochemical tests, including cyclic voltammetry (CV) and electrochemical impedance spectroscopy (EIS, a frequency range from 100 kHz to 0.1 Hz at 0.4 V), were conducted with a CHI 660D electrochemical workstation using a three-electrode setup in 1 M NaCl electrolyte. The working electrode is composed of active material (m-PTPA or n-PTPA or active carbon), carbon black, and polyvinylidene fluoride with a mass ratio of 8:1:1. The Pt and Ag/AgCl were applied as the counter electrode and reference electrode, respectively. The specific capacitance (C, F g^{-1}) of an electrode material can be calculated using the following formula[4]

$$C = \frac{\int I \cdot \mathrm{d}E}{2v \cdot m \cdot \Delta E} \qquad (1)$$

where I (mA), v (mV s^{-1}), ΔE, and m (g) represent the corresponding current, scan rate, potential window, and the mass of active materials, respectively.

Desalination performances of m-PTPA or n-PTPA were tested by a typical CDI device shown in Figure S7. The preparation method of CDI electrodes is the same as that of the working electrode for electrochemical experiments, but using 2~12 mg cm^{-2} active materials on each electrode with a geometric area of 3 × 3 cm^2. During the desalination process, saline solution (50 mL) was recirculated through the CDI device with a rate of 25 mL min^{-1} at room temperature. The electrochemical workstation (CHI 660E) is used to apply a DC voltage to the parallel electrodes, and to simultaneously measure the current response versus time. A conductivity/pH meter (Seven Excellence Cond meter) was immersed in the saline solution to measure the variation of conductivity and pH versus time. Accordingly, Gravimetric/areal/volumetric salt adsorption capacity (SAC$_{grav}$, mg g^{-1}; SAC$_{areal}$, mg cm^{-2}; SAC$_{volum}$, mg cm^{-3}), average salt adsorption rate (ASAR), energy consumption (EC), and charge efficiency (CE) were calculated based on the following equations:[5, 6]

$$SAC_{grav} = \frac{(c_0 - c) \cdot V}{m} \qquad (2)$$

$$SAC_{areal} = \frac{(c_0 - c) \cdot V}{A} \qquad (3)$$

$$SAC_{volum} = \frac{(c_0 - c) \cdot V}{A \cdot T} \qquad (4)$$

$$ASAR = \frac{SAC_{grav}}{t} \qquad (5)$$

$$EC = \frac{E \cdot \int i \cdot dt}{3600 \cdot (c_0 - c) \cdot V \cdot M_{NaCl}} \qquad (6)$$

$$CE = \frac{(c_0 - c) \cdot V \cdot F}{\int i \cdot dt} \times 100\% \qquad (7)$$

where c_0 and c (mol L^{-1}) are the initial and final concentration of the saline solution, respectively; V (L) is total volume of the saline solution; E (V) is the applied voltage during desalination process; i (A) is the current during desalination process; t (s) is the CDI time; A (cm^2) and T (cm) are the geometric area and thickness of electrode; and M_{NaCl} is the molar mass of NaCl (58.5 g mol^{-1}).

According to Equations (2)-(4), SAC_{grav} indicates the mass of salt removed by per mass of electrode (yielding a unit of mg g^{-1}), SAC_{areal} (mg cm^{-2}) and SAC_{volum} (mg cm^{-3}) indicate the mass of salt removed by per areal and volume of electrode respevtively. The reason for the usage of them in the work lies in two considerations. On the one hand, SAC_{grav} is a routine presentation for characterizing CDI performance of electrode materials, and can be used for making a rough comparison between differnt materials. On the other hand, SAC_{areal} and SAC_{volum} are in close relation to electrode preparations (e.g. mass loadings and/or thicknesses of the electrode material), which can give additional insight into the performance of an electrode material.[7] Electrode materials with large SAC_{areal} or SAC_{volum} are highly

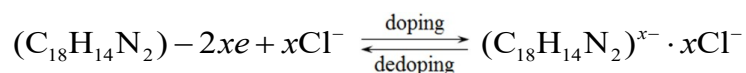appreciated both for the development of new materials and for the minimization of CDI devices.

Calculation detail: Density function theory (DFT) calculations were performed for the structural optimization and energy estimation based on DMol^3 package.[8] The Perdew-Burke-Ernzerhof (PBE) exchange-correlation functional of generalized gradient approximation (GGA) was adopted to describe exchange-correlation functional.[9] For structure optimization an energy calculations, the convergence tolerance was set as 1.0×10^{-5} Ha, 0.002 Ha Å^{-1}, and 0.05 Å for energy, maximum force, and maximum displacement, respectively. The Cl$^-$-PTPA structural models, M-Cl, M-2Cl, M-3Cl, M-4Cl, which represent different doping levels (25, 50, 75 and 100%), were constructed with a PTPA molecular fragment and 1-4 Cl$^-$ ions (Figure S15). The initial N−Cl atomic distances between Cl$^-$ ion and N atom in PTPA was set as ~2.5 Å, which corresponds to the sum of the ionic radius of Cl$^-$ (1.81 Å) and covalent radius of N atom (0.70 Å).[10] The adsorption energy (ΔE) was calculated using the equation:

$$\Delta E = E_{\text{Cl-PTPA}} - E_{\text{PTPA}} - E_{\text{Cl}} \qquad (8)$$

where $E_{\text{Cl-PTPA}}$, E_{PTPA}, and E_{Cl} are the energies of Cl$^-$-PTPA model molecule, PTPA molecule, and Cl$^-$ ion, respectively.

Note I: Estimation for the Cl⁻ dopant concentration of $x \approx 0.25$.

With the measured maximum salt adsorption capacity (SAC) of ~50 mg g^{-1} (Figure 4f) and ~60 mg g^{-1} (Figure 4c), we calculated the Cl⁻ dopant concentration. The anodic reaction for Cl⁻ doping in PTPA is

$$(C_{18}H_{14}N_2) - 2xe + xCl^- \underset{\text{dedoping}}{\overset{\text{doping}}{\rightleftharpoons}} (C_{18}H_{14}N_2)^{x-} \cdot xCl^-$$

The physical meaning of SAC = 50 mg g^{-1} is 50 mg NaCl adsorbed by per gram of PTPA. The molecular mass of NaCl and the elementary unit of PTPA ($C_{18}H_{14}N_2$) is 58.5 and 258 g mol^{-1}, respectively.

50 mg NaCl = 50/58.5 = 0.855 mmol NaCl = 0.855 mmol Cl⁻

1 g PTPA = 1/258 = 3.88×10^{-3} mol PTPA = 3.88 mmol PTPA

So, the dopant concentration is x = (0.855 mmol Cl⁻) / (3.88 mmol PTPA) = 0.220.

Similarly, x = 0.264 was estimated for SAC = 60 mg g^{-1}.

As a result, we regard the experimental value as $x \approx 0.25$ in this work, i.e., about 0.2 Cl⁻ ion was captured by per ($C_{18}H_{14}N_2$) constitutional unit of PTPA.
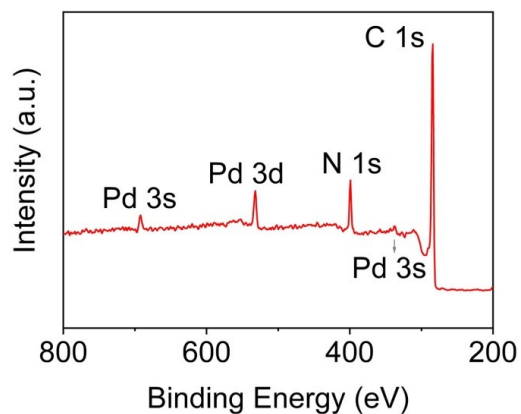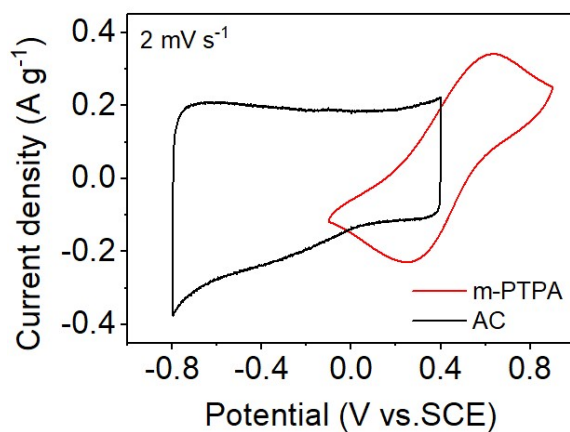
Figure S1. XPS spectrum for m-PTPA.

Figure S2. CV curves of AC and m-PTPA measured at 2 mV s^{-1}, showing an operable 1.6 V wide voltage window (from -0.8 to 0.8 V) for constructing an HCDI desalination cell composed of m-PTPA anode and AC cathode.
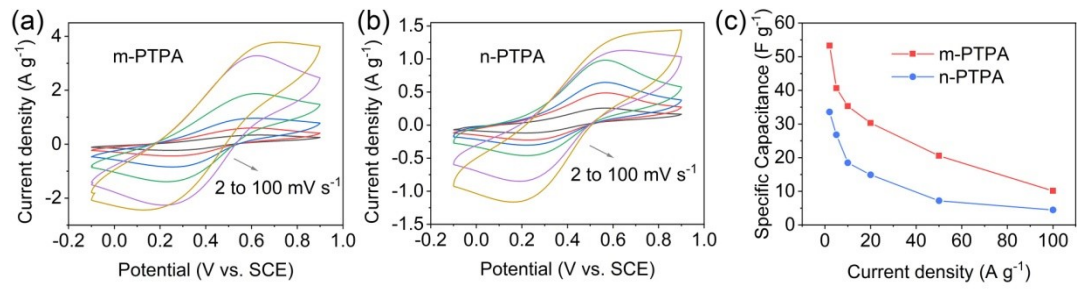
Figure S3. CV curves of (a) m-PTPA and (b) n-PTPA at various scan rates. (c) Comparison of specific capacitances vs different scan rates.
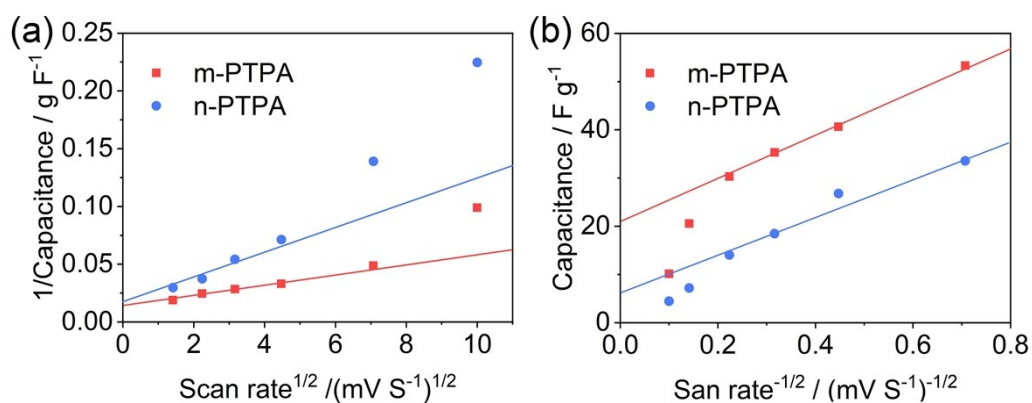
Figure S4. (a) The relationship of specific capacitance versus inverse square root of scan rate and (b) the relationship of inverse specific capacity versus square root of scan rate for the n-PTPA and m-PTPA electrodes.

The surface- and diffusion-controlled processes can be distinguished by their capacitive responses under different scan rates (Figure S3). The surface-controlled processes would dominate the capacitive response at high scan rates due to the insufficient time for the ions to diffuse into the inner surface of the electrode, and vice versa for the diffusion-controlled processes at low scan rates. So, based on Trasatti equations, $C^{-1} = C_{tot} + \text{constant} \cdot v^{1/2}$ and $C = C_{edl} + \text{constant} \cdot v^{-1/2}$, the total capacitance (C_{tot}) and the contribution of surface-controlled process (C_{edl}) can be estimated from the C^{-1} versus $v^{1/2}$ plot at $v \rightarrow 0$ (Figure S4a) and C versus $v^{-1/2}$ plot at $v \rightarrow \infty$ (Figure S4b), respectively. Then, the difference between C_{tot} and C_{edl} gives the contribution of diffusion-controlled process (C_{diff}).
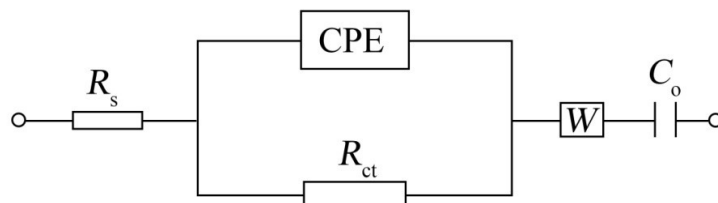
Figure S5. Equivalent electrical circuit model used for fitting the measured EIS spectra (Figure 3c). Here, R_s is the uncompensated solution resistance, CPE is constant phase element representing the surface double layer capacitance ($Z_{CPE} = Y_0^{-1} \cdot (j\omega)^{-n}$), R_{ct} is the charge transfer resistance, W is the Warburg diffusion element ($Z_W = \sigma/\sqrt{\omega} - j \cdot \sigma/\sqrt{\omega}$), and C_0 is the low-frequency limiting capacitance.
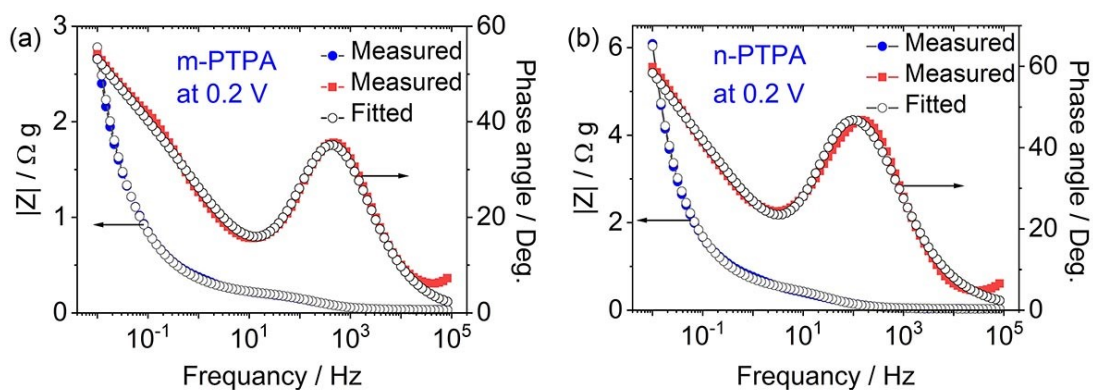

Figure S6. Measured and fitted Bode |Z| and Bode phase plots of m-PTPA (a) and n-PTPA (b).
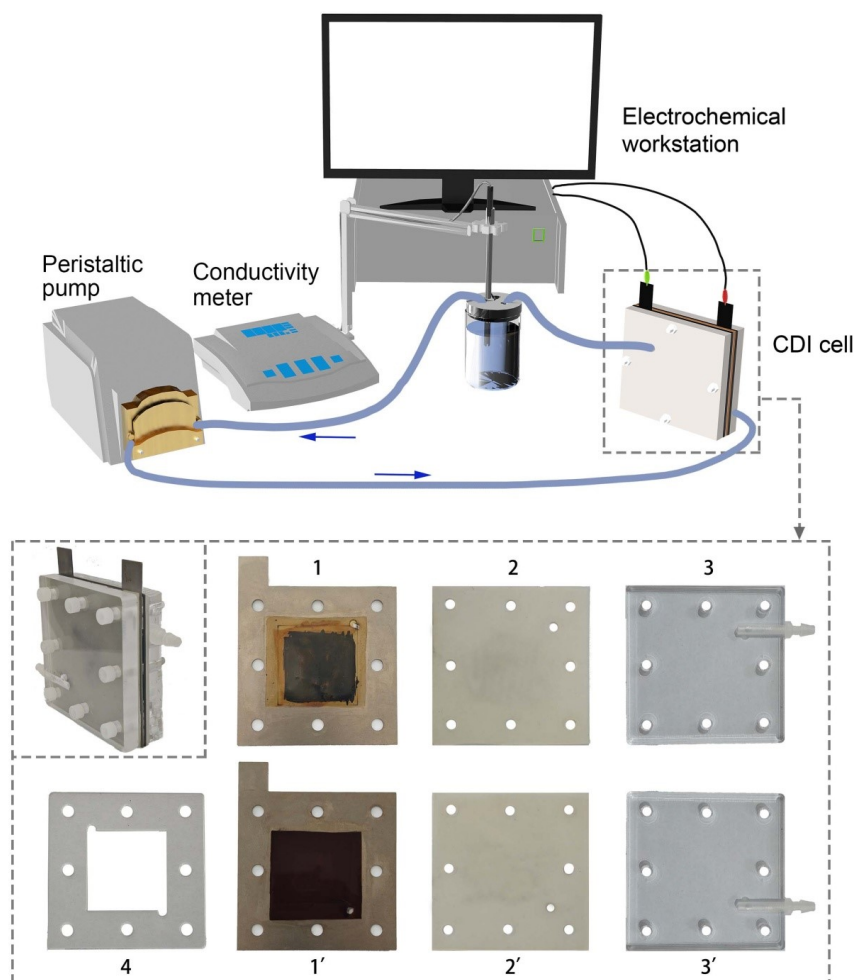
Figure S7. Schematics showing the CDI device and the CDI cell. The CDI cell is made of (1, 1') CDI electrodes, (2, 2') silicon rubber slice, (3, 3') plexiglas plate, and (4) silicon rubber spacer.
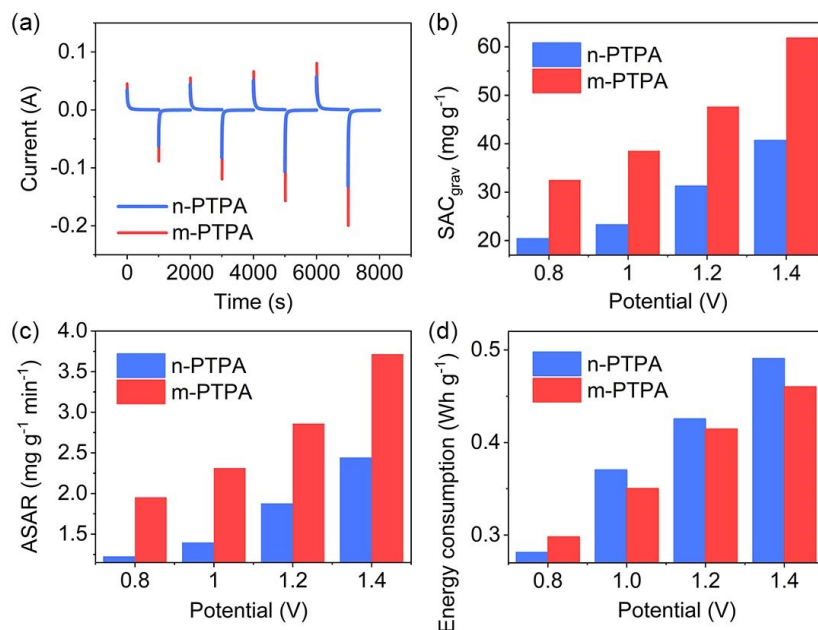
Figure S8 (a) The the current response versus CDI time for the m-PTPA‖AC and n-PTPA‖AC cells at different voltage with the initial concentration of 500 mg L^{-1}. The corresponding (b) SAC, (c) adsorption rate, and (d) energy consumption for the m-PTPA‖AC and n-PTPA‖AC cells.

As the varied applied voltage from ±0.8 to ±1.4 V, the conductivity of the NaCl solution decreased sharply upon the application of a voltage bias and returned fast to its initial value once the voltage was removed (Figure 4a), indicating a satisfactory reversibility for the salt adsorption-desorption processes within both m-PTPA and n-PTPA elctrodes.[11] Meanwhile, the regular current-time curves indicate no undesirable Faradaic reactions generate during the adsorption-desorption process, even at 1.4 V (Figure S8a).[12] Accordingly, the SAC$_{grav}$, adsorption rate, and energy consumption increase almost linearly with the applied voltage, i.e., from 32.5 mg g^{-1}, 1.95 mg g^{-1} min^{-1}, and 0.19 Wh g^{-1} at 0.8 V to 61.9 mg g^{-1}, 3.71 mg g^{-1} min^{-1}, and 0.326 Wh g^{-1} at 1.4 V for the m-PTPA‖AC cell (Figure S8b-d).
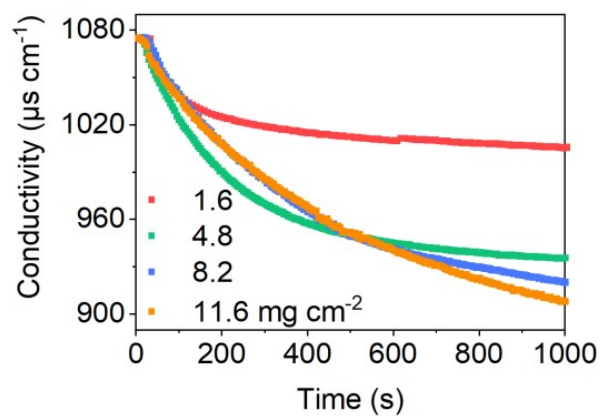
Figure S9. The conductivity variation of the NaCl solution versus CDI time for the n-PTPA‖AC cell with different mass loading.
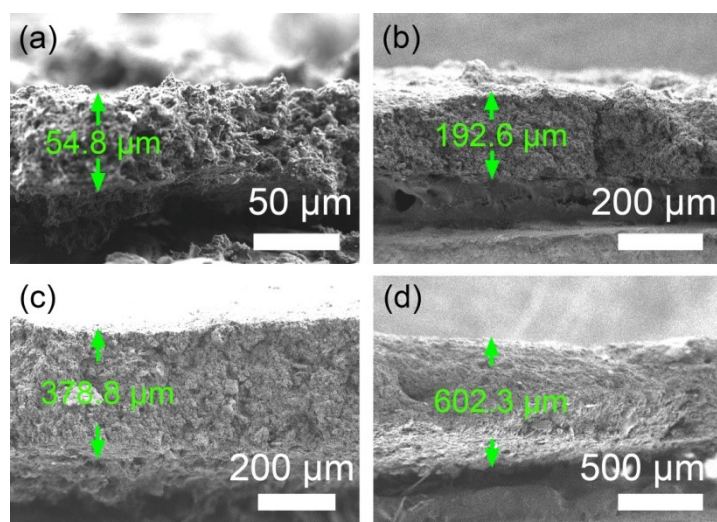
Figure S10. The coss-sectional SEM images for the m-PTPA electrodes with different mass loading of 1.7, 4.7, 8.7, and 11.7 mg cm^{-2}.
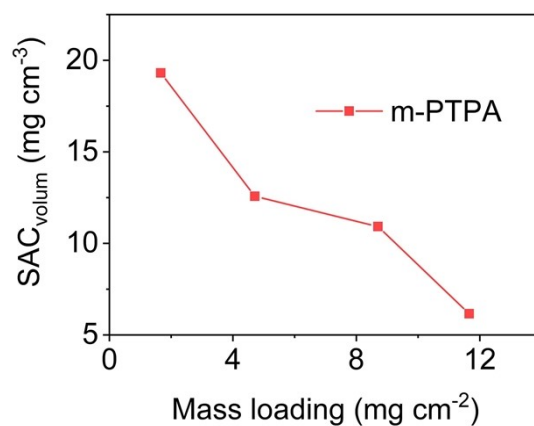
Figure S11. The volumetric-SAC for m-PTPA||AC cells with different mass loading.
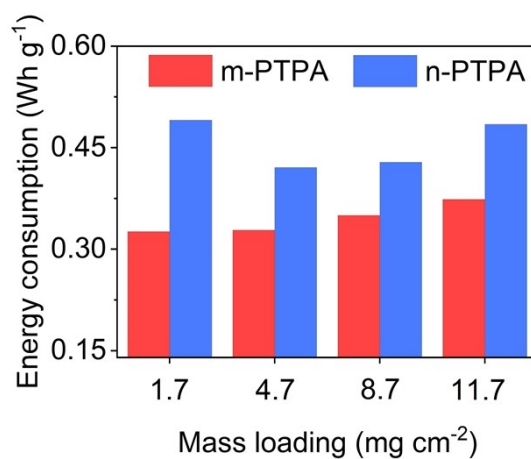
Figure S12. The energy consumption for m-PTPA||AC and n-PTPA||AC cells with different mass loading.
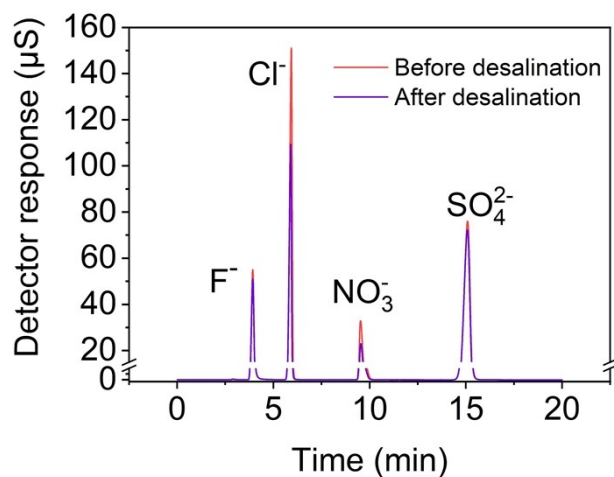
Figure S13. The comparison of chromatograms of Cl^-, F^-, NO_3^-, and SO_4^{2-} on anion exchange column before and after desalination process using the m-PTPA‖AC cell.
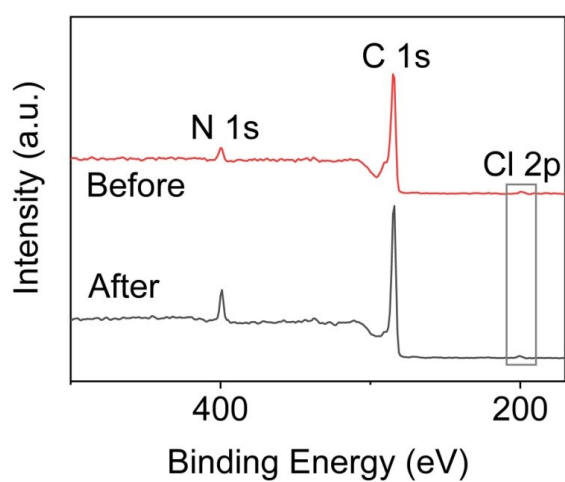
Figure S14. XPS spectra of m-PTPA after adsorption and desorption process.
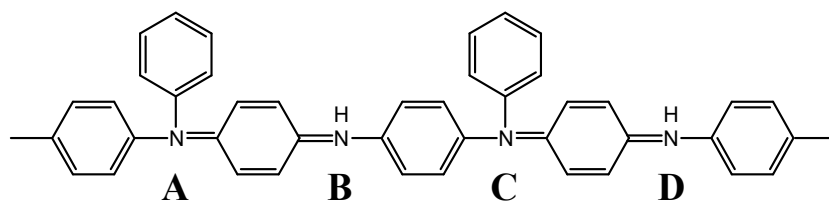
Figure S15. PTPA molecular fragment with four N atom sites for adsorbing Cl⁻ ions, two TPA N atoms (A and C sites), and two bridging N atoms (B and D sites). Accordingly, the Cl⁻ adsorption models for DFT calculations were constructed by placing 1-4 Cl⁻ ions at the N atom sites with an initial N−Cl atomic distance of ~2.5 Å. The model M-Cl and M-Cl' is formed with 1 Cl⁻ at A and B site, respectively (doping level 25%); M-2Cl is with 2 Cl⁻ at A and C sites (50%); M-3Cl is with 3 Cl⁻ at A, B and C sites (75%); M-4Cl is with 4 Cl⁻ at A, B, C and D sites (100%).
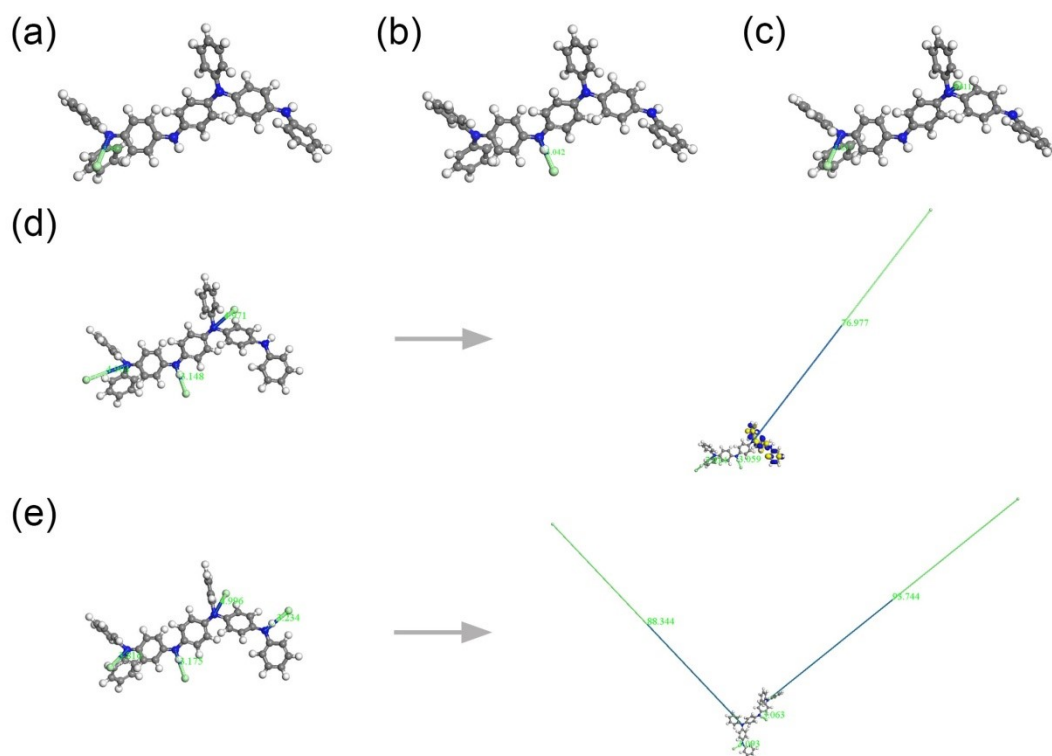
Figure S16. Optimized structures for (a) M-Cl (doping level 25%), N−Cl distance 3.585 Å; (b) M-Cl' (doping level 25%), N−Cl distance 3.042 Å; (c) M-2Cl (doping level 50%), N−Cl distance 3.611 and 3.637 Å; (d) M-3Cl (doping level 75%), N−Cl distance 3-5 Å in a transition state (left) and one N−Cl distance 77.0 Å in final state (right); (e) M-4Cl (doping level 100%), N−Cl distance 3-5 Å in a transition state (left) and two N−Cl distance 88.3 and 93.7 Å in final state (right).

Table S1. Summary of specific surface area, pore volume, and pore diameter of n-PTPA and m-PTPA.

Electrode materials	BET surface area $(m^2\,g^{-1})$	Langmuir surface area $(m^2\,g^{-1})$	Microporous surface area $(m^2\,g^{-1})$ [a]	Mesoporous surface area $(m^2\,g^{-1})$	Total pore volumes $(cm^3\,g^{-1})$ [b]	Microporous volume $(cm^3\,g^{-1})$ [c]	Mesoporous volume $(cm^3\,g^{-1})$
n-PTPA	58.2	66.5	52.8	13.7	0.060	0.019	0.034
m-PTPA	506.1	647.8	591.4	56.4	0.320	0.210	0.080

[a] Estmated by DR method;

[b] Estmated at $P/P_0 = 0.93$;

[c] Estmated by DR method;

[d] Single point average pore diameter.

Table S2. Electrochemical parameter values estimated for m-PTPA and n-PTPA by equivalent electrical circuit fitting (**Figure S6**).

	R_s / Ω g	Q-Y_0 / F g^{-1} s^{n-1}	Q-n	R_{ct} / Ω g	σ / Ω $s^{-1/2}$	C_0 / F g^{-1}
m-PTPA	0.031	0.027	0.815	0.142	0.374	21.85
n-PTPA	0.030	0.043	0.849	0.338	0.700	6.79

Table S3. A summary of desalination performance of anode materials for anion capture in CDI.

Materials †	Mass loading (mg cm^{-2})	NaCl concentration (mg L^{-1})	Cell voltage (V) or Current density	Gravimetric-SAC (mg g^{-1})	Areal-SAC (mg cm^{-2})	Volumetric-SAC (mg cm^{-3})	Average salt adsorption rate (mg g^{-1} min^{-1})	Ref
Polymer-based materials								
m-PTPA	8.7	500	1.4	47.21	0.4137	10.92	2.832	This work
n-PTPA	8.2	500	1.4	26.85	0.2261	5.968	1.611	This work
Polypyrrole/ZIF-67	10	584 / 1530	1.2	11.34 / 15.3			0.378 / 0.255	13
Poly-p-phenylene	1.25	2500 / 500	1.8	41.9 / 17.2	0.0655 / 0.0269		1.27 / 0.52	12
Polyaniline/AC	14.3	250	1.2	3.15	0.045		0.105	14

Polyaniline@carbon	23.2	1500~1700	1.2	14.1	0.327		0.47	15
PTMA	1.563	250	1.2	20.9	0.03266	4.665	0.6967	16

Carbon-based materials

Carbon fibers	36	1750	1.2	9.44	0.34	4.25	0.31	17
	72			8.33	0.6	3.75	0.28	
	108			7.14	0.76	3.04	0.238	
3D graphene framework	16.8	50	1.6	1.98	0.033		0.033	18
		500		3.45	0.058		0.058	
Carbon fiber paper	20.6	50	1.2	0.59	0.0122	0.61	0.0098	6
		3500		1.94	0.04	2	0.032	
Porous carbon fibers cloth-900	12.5	100	1.2	2.28	0.029	0.8788	0.076	19
Porous carbon fibers cloth-1000	12.5	100	1.2	2.96	0.037	1.121	0.09867	

Porous carbon fibers cloth/CNTs	12.5	100	1.2	3.40	0.051	1.545	0.1133	
Carbon nanofibers		500	2	18.27	0.0817	2.14	3.32	20
Wood-derived carbon	50	100	1.2	5.7	0.3	2.4	0.03167	21
Polyacrylonitrile-drived carbon fiber	8.86	96	1.6	4.64	0.041	2.05	0.029	22
N-doped rGO/carbon nanofibers	4.48	50	1.2	3.92	0.0175			23
Ultra-thin carbon nanofiber networks	6.25	200 1000	1.2	6.72 12.81	0.042 0.08	1.68 3.2	0.168 0.32	24
Porous carbon nanofibers	3.5	500	1.2	8.1	0.029		1.013	25
Holey graphene foam	2	572	2.0	29.6	0.06	0.023	0.9867	26
Free-standing AC	55	1000 250	1.2	8.9 3	0.49 0.16	2.48 0.83	0.127 0.025	27

Material								
Mesoporous carbon nanofiber fabric	3	500	1.2	19.3	0.021		0.71	28
Lotus stems-drived carbon	3.11~3.89	500	1.4	31.7	0.0986~0.123	2.53~3.16	3.9	29
Graphene hollow carbon spheres	16.67	34	1.6	2.3	0.038	1.28	0.019	30
N, P, S co-doped hollow carbon	3.97	500	1.2	22.19	0.088	8.8	0.1849	31

Some other materials

Material								
Porous $Ti_3C_2T_x$ MXene	1.0	10000	1.2	45		118	2.81	32
N-doped $Ti_3C_2T_x$		5000	1.2	43.5		117		33
MoS_2/N-doped carbon		250	1.6	28.82			0.48	34
MoS_2/CNT		29250	0.8	25		125	0.417	35

TiO$_2$/carbon	25 23.97	280	1.2	17.4 11.4	0.44 0.27	22~24.4 15~13.5	0.58 0.38	36
TiO$_2$/rGO	8.3	300	1.2	16.4	0.1361	8.05	3.28	37
BiOCl@G	1.11	500 1500	1.4	50.0 61.6	0.056 0.068		3 3.72	38
BiOCl/C fiber	7.5	3000	500 mA g^{-1}	62	0.465	23.25	10.8	39
Bi/C fiber	3.33	3000	220 mA g^{-1}	51.13	0.17		4.32	40
BiOCl	1.25	740	100 mA g^{-1}	69.18	0.086	4.32	1.14	39
Ag/AC	15.9	585	1.2	23.3	0.35	23.5	2.328	41
CoFe LDH	8.97	600	1.2	34.2	0.31		0.228	42
Co/N-doped C	1.5	824	1.4	58.82	0.088	8.8		43

Co/N-doped C	4.08	1000	1.2	55.6	0.23	1.236	44
ZnCo-Cl LDH	0.79	500	1.2	56.1	0.085	0.936	45
Fe$_2$O$_3$/Red oak drived C	5.8	200	1.2	13.79	0.08	0.4596	46

† **Note for abrievations.**

ZIF: zeolitic imidazolate framework

AC: activated carbon

PTMA: Poly (2,2,6,6-tetramethylpiperidinyloxy methacrylate)

CNTs: The carbon nanotubes

Table S4. Intrinsic properties for the studied anions.[†]

Ion	Hydrated radius / nm	Diffusion coefficient / $cm^2\ s^{-1}$	Ion formation Gibbs Energy / $kJ\ mol^{-1}$
F^-	0.352	1.48×10^{-5}	-278.8
Cl^-	0.332	2.03×10^{-5}	-131.3
NO_3^-	0.335	1.90×10^{-5}	-111.3
SO_4^{2-}	0.379	1.07×10^{-5}	-744.5

[†] Data from (1) E.R. Nightingale Jr., J. Phys. Chem., 63 (1959) (9) 1381-1387

(2) A.G. Volkov, S. Paula, D.W. Deamer, Bioelectrochem. Bioenerg., 42 (1997) (2) 153-160

(3) CRC Handbook of Chemistry and Physics, 84th Edition, Edited by D.R. Lide, CRC Press LLC, 2004

Table S5. Binding energies and relative atomic contents of chemical groups/species estimated from core level XPS spectra of N 1s, C 1s and Cl 2p for m-PTPA electrode before and after anodic oxidation.

Groups	Before oxidation/adsorption		After oxidation/adsorption		Core level spectra
	Peak position / eV	Relative contents / at.%	Peak position / eV	Relative contents / at.%	
−NR−/−NH−	399.99	93.87	400.10	47.3	N 1s
−NR$^+$−	401.15	6.13	400.90	20.2	
−N=		0	398.40	11.1	
−NR$^+$=		0	402.50	21.4	
C=C	284.64	74.7	284.72	43.1	C 1s
C−N	285.56	25.3	285.61	32.7	
C=N		0	287.00	24.2	
Cl$^-$	198.00	34.6	198	18.1	Cl 2p
N$^+$−Cl$^-$	200.35	45.6	200.31	56.6	
C−Cl	202.00	19.8	202.01	25.3	

References

1. Y. Z. Liao, J. Weber and C. F. J. Faul, *Chem. Commun.*, 2014, **50**, 8002-8005.
2. J. Chen, W. Yan, E. J. Townsend, J. T. Feng, L. Pan, V. D. Hernandez and C. F. J. Faul, *Angew. Chem. Int. Ed.*, 2019, **58**, 11715-11719.
3. X. Y. Yang, H. L. Jiang, W. W. Zhang, T. Liu, J. Bai, F. Guo, Y. Yang, Z. C. Wang and J. F. Zhang, *Sep. Purif. Technol.*, 2021, **276**, 119379.
4. W. Kong, X. Duan, Y. Ge, H. Liu, J. Hu and X. Duan, *Nano Res.*, 2016, **9**, 2458-2466.
5. W. Q. Kong, X. Ge, D. S. Kong, C. M. Liu, J. P. Sun, X. Zhu, M. Zhang and Y. Y. Feng, *Desalination*, 2024, **573**, 117222.
6. W. Q. Kong, G. Wang, M. Zhang, X. D. Duan, J. W. Hu and X. F. Duan, *Desalination*, 2019, **459**, 1-9.
7. M. E. Suss, S. Porada, X. Sun, P. M. Biesheuvel, J. Yoon and V. Presser, *Energy Environ. Sci.*, 2015, **8**, 2296-2319.
8. B. Delley, *J. Chem. Phys.*, 2000, **113**, 7756-7764.
9. J. P. Perdew, K. Burke and M. Ernzerhof, *Phys. Rev. Lett.*, 1996, **77**, 3865.
10. J. G. Speight, *Lange's handbook of chemistry*, McGraw-Hill New York, 2005.
11. M. Ding, S. Li, L. Guo, L. Jing, S. P. Gao, H. T. Yang, J. M. Little, T. U. Dissanayake, K. R. Li, J. Yang, Y. X. Guo, H. Y. Yang, T. J. Woehl and P. Y. Chen, *Adv. Energy Mater.*, 2021, **11**, 2101494.
12. W. Q. Kong, X. Ge, M. Q. Yang, Q. A. Zhang, J. Y. Lu, H. K. Wen, H. Y. Wen, D. S. Kong, M. Zhang, X. Zhu and Y. Y. Feng, *Desalination*, 2023, **553**, 116452.
13. Z. M. Wang, X. T. Xu, J. Kim, V. Malgras, R. Mo, C. L. Li, Y. Z. Lin, H. B. Tan, J. Tang, L. K. Pan, Y. Bando, T. Yang and Y. Yamauchi, *Mater. Horizons*, 2019, **6**, 1433-1437.
14. C. J. Yan, L. D. Zou and R. Short, *Desalination*, 2014, **333**, 101-106.
15. S. F. Evans, M. R. Ivancevic, D. J. Wilson, Z. D. Hood, S. P. Adhikari, A. K. Naskar, C. Tsouris and M. P. Paranthaman, *Desalination*, 2019, **464**, 25-32.
16. Y. Q. Li, Z. B. Ding, J. B. Li, K. Wang, T. Lu and L. K. Pan, *Desalination*, 2020, **481**, 114379.
17. C. J. Zhang, D. Wang, Y. Qiu, Q. Zhang, Z. Y. Liu, Y. A. Liu, J. Hu and G. W. Wen, *Chem. Eng. J.*, 2023, **471**, 144526.
18. Q. L. Liu, X. Q. Li, G. Q. Tan and D. Xiao, *Desalination*, 2022, **538**, 115890.
19. C. J. Zhang, D. Wang, Z. Wang, G. S. Zhang, Z. C. Liu, J. Wu, J. Hu and G. W. Wen, *Energy Environ. Mater.*, 2023, **6**, e12276.
20. L. H. Yin, P. Y. Hu, C. Liang, J. Wang, M. Li and W. D. Qu, *Int. J. Biol. Macromol.*, 2023, **225**, 1415-1425.
21. M. Q. Liu, M. Xu, Y. F. Xue, W. Ni, S. L. Huo, L. L. Wu, Z. Y. Yang and Y. M. Yan, *ACS Appl. Mater. Interfaces*, 2018, **10**, 31260-31270.
22. G. Wang, C. Pan, L. P. Wang, Q. Dong, C. Yu, Z. B. Zhao and J. S. Qiu, *Electrochim. Acta*, 2012, **69**, 65-70.

23. Y. Liu, X. T. Xu, T. Lu, Z. Sun, D. H. C. Chua and L. K. Pan, *RSC Adv.*, 2015, **5**, 34117-34124.

24. Y. Liu, T. Lu, Z. Sun, D. H. C. Chua and L. K. Pan, *J. Mater. Chem. A*, 2015, **3**, 8693-8700.

25. H. J. Pan, J. M. Yang, S. P. Wang, Z. B. Xiong, W. S. Cai and J. Y. Liu, *J. Mater. Chem. A*, 2015, **3**, 13827-13834.

26. J. Li, B. X. Ji, R. Jiang, P. P. Zhang, N. Chen, G. F. Zhang and L. T. Qu, *Carbon*, 2018, **129**, 95-103.

27. L. L. Wu, M. Q. Liu, S. T. Huo, X. G. Zang, M. Xu, W. Ni, Z. Y. Yang and Y. M. Yan, *Carbon*, 2019, **149**, 627-636.

28. X. Y. Gong, S. Zhang, W. X. Luo, N. N. Guo, L. X. Wang, D. Z. Jia, Z. B. Zhao, S. Z. Feng and L. X. Jia, *ACS Appl. Mater. Interfaces*, 2020, **12**, 49586-49595.

29. X. M. Ma, Q. H. Wu, W. Wang, S. F. Lu, Y. Xiang and D. Aurbach, *J. Mater. Chem. A*, 2020, **8**, 16312-16322.

30. H. Wang, L. Y. Shi, T. T. Yan, J. P. Zhang, Q. D. Zhong and D. S. Zhang, *J. Mater. Chem. A*, 2014, **2**, 4739-4750.

31. J. Zhang, J. H. Fang, J. L. Han, T. T. Yan, L. Y. Shi and D. S. Zhang, *J. Mater. Chem. A*, 2018, **6**, 15245-15252.

32. W. Z. Bao, X. Tang, X. Guo, S. Choi, C. Y. Wang, Y. Gogotsi and G. X. Wang, *Joule*, 2018, **2**, 778-787.

33. A. Amiri, Y. J. Chen, C. B. Teng and M. Naraghi, *Energy Storage Mater.*, 2020, **25**, 731-739.

34. S. C. Tian, X. H. Zhang and Z. H. Zhang, *Chem. Eng. J.*, 2021, **409**, 128200.

35. P. Srimuk, J. Lee, S. Fleischmann, S. Choudhury, N. Jäckel, M. Zeiger, C. Kim, M. Aslan and V. Presser, *J. Mater. Chem. A*, 2017, **5**, 15640-15649.

36. P. Srimuk, M. Zeiger, N. Jäckel, A. Tolosa, B. Krüner, S. Fleischmann, I. Grobelsek, M. Aslan, B. Shvartsev, M. E. Suss and V. Presser, *Electrochim. Acta*, 2017, **224**, 314-328.

37. A. G. El-Deen, J. H. Choi, C. S. Kim, K. A. Khalil, A. A. Almajid and N. A. M. Barakat, *Desalination*, 2015, **361**, 53-64.

38. Y. Liu, X. Gao, Z. P. Wang, K. Wang, X. Y. Dou, H. G. Zhu, X. Yuan and L. K. Pan, *Chem. Eng. J.*, 2021, **403**, 126326.

39. L. H. Wang, Z. Z. Liu, Z. P. Wang, Q. H. Ma, Z. X. Guo, G. Z. Shen, K. Wang, X. T. Xu, Y. Liu and X. Yuan, *Chem. Eng. J.*, 2023, **460**, 141726.

40. D. C. Han, S. Y. Wang, C. M. Zhang, R. Y. Yue, S. G. Wang and X. F. Sun, *Electrochim. Acta*, 2022, **436**, 141380.

41. H. Yoon, J. Lee, T. Min, G. Lee and M. Oh, *Environ. Sci.: Water Res. Technol.*, 2021, **7**, 1315-1321.

42. Z. Li, S. D. Mao, Y. Yang, Z. Sun and R. Zhao, *J. Colloid Interface Sci.*, 2021, **585**, 85-94.

43. X. X. Hu, X. B. Min, H. Y. Wang, X. Y. Li, Y. H. He and W. C. Yang, *Sep.*

Purif. Technol., 2021, **266**, 118590.

44. S. L. Huo, W. Ni, Y. F. Zhao, X. Song, Y. B. Zhao, K. X. Li, H. Wang and M. T. Zhang, *J. Mater. Chem. A*, 2021, **9**, 3066-3076.

45. Z. H. Zhang and H. B. Li, *Environ. Sci.: Nano*, 2021, **8**, 1886-1895.

46. Z. Y. Du, W. J. Tian, K. L. Qiao, J. Zhao, L. Wang, W. L. Xie, M. L. Chu and T. T. Song, *Sep. Purif. Technol.*, 2020, **233**, 116024.